Research Article Vol. 13, No. 1 / 1 Jan 2022 / Biomedical Optics Express 237
Biomedical Optics EXPRESS

F-CUBIC: a rapid optical clearing method optimized by quantitative evaluation

LINA LIU,[1,2,4] XIANYUAN XIA,[1,2,4] FENG XIANG,[1,2] YUFENG GAO,[1,2] XI LI,[3] HUI LI,[1,2,5] AND WEI ZHENG[1,2,6]

[1]*Research Center for Biomedical Optics and Molecular Imaging, Shenzhen Key Laboratory for Molecular Imaging, Guangdong Provincial Key Laboratory of Biomedical Optical Imaging Technology, Shenzhen Institute of Advanced Technology, Chinese Academy of Sciences, Shenzhen 518055, China*
[2]*CAS Key Laboratory of Health Informatics, Shenzhen Institute of Advanced Technology, Chinese Academy of Sciences, Shenzhen 518055, China*
[3]*Department of Gastroenterology, Peking University Shenzhen Hospital, Shen Zhen 518036, China*
[4]*Authors contributed equally to this work*
[5]*hui.li@siat.ac.cn*
[6]*zhengwei@siat.ac.cn*

Abstract: In recent decades, various powerful optical clearing methods have emerged to facilitate deep-tissue imaging. However, a rapid and safe protocol for millimeter-thick specimens is still desired. In this study, we propose a simple and economical chemical screening method that uses porcine small intestine tissue as the testing sample to quantify the clearing speed of different optical clearing reagents. By screening with this method, we developed a fast and versatile clearing protocol, termed F-CUBIC (adding formamide to CUBIC). F-CUBIC allows easy clearing of millimeter-thick tissues within 2–20 min by one-step immersion at room temperature. It introduces negligible tissue distortion and shows high compatibility with various fluorescent labeling techniques. Based on endoscopic human colon specimens, we successfully demonstrated the potential of F-CUBIC for nondestructive three-dimensional (3D) biopsy in combination with two-photon microscopy. This study would substantially benefit rapid 3D tissue mapping in biomedical research and clinics, such as instant histopathological examinations.

1. Introduction

Rapidly obtaining three-dimensional (3D) morphological information of tissues or organs with millimeter-scale thickness at subcellular resolution provides great value in biomedical research and clinical applications. Novel optical sectioning imaging techniques, such as multiphoton microscopy and light-sheet fluorescence microscopy, have provided considerable advances in performing rapid noninvasive 3D imaging [1–3]. However, their imaging penetration depth is restricted by the effects of scattering and absorption arising from biological tissues [4]. Recently developed optical clearing techniques can substantially reduce tissue scattering and absorption by unifying the refractive index (RI) inside the sample and removing endogenous absorbents, enabling an improved depth imaging of biological tissues [4–9]. However, some limitations such as slow speed, complexity, and toxicity have restricted the wide use of optical clearing process in biomedical and clinical applications.

To date, various optical clearing techniques have been developed. These techniques are generally categorized into organic solvent- or aqueous solution-based methods [5,10,11]. Organic solvent-based methods such as 3DISCO [12] can achieve a high level of tissue transparency and a favorable clearing speed [10,13,14]. However, they usually suffer from severe fluorescence quenching [10,13,14]. Although the latest methods, including uDISCO [15], vDISCO [16], sDISCO [17], and FDISCO [18] partially alleviate this issue, the toxicity of organic solvents to operators and the environment still restricts their widespread use [10].

#442976 https://doi.org/10.1364/BOE.442976
Journal © 2022 Received 10 Sep 2021; revised 20 Nov 2021; accepted 23 Nov 2021; published 7 Dec 2021

Biomedical Optics EXPRESS

In contrast, aqueous solution-based methods provide good fluorescence preservation with low toxicity [10,13,14]. Aqueous clearing is further classified into simple immersion and hydrogel embedding techniques [10]. Compared with the hydrogel-embedding techniques that require time-consuming and cumbersome steps (such as CLARITY [19,20] and PACT [21]), simple immersion methods are more popular owing to their ease. Sca*l*e series are the most representative immersion methods that have extended the imaging depth to several millimeters in the adult mouse brain [22]. However, the prolonged incubation upto several days [22], is a major limitation. After Sca*l*e, methods that shorten the clearing time have been developed, such as $Clear^{T/T2}$ [23], SeeDB/SeeDB2 [24,25], CUBIC [26,27], FRUIT [28], UbasM [29], RTF [30], FOCM [31], Sca*l*eS [32], and MACS [11]. Among these methods, the CUBIC presented by rescreening the chemical components of Sca*l*eA2 is known for its rapid and efficient clearing ability and favorable fluorescence compatibility [26]. Therefore, the CUBIC method has been widely used and adequately optimized for different purposes [5] (for example, CUBIC-L [33] for delipidation, CUBIC-X [34] for tissue expansion, *etc*.). Despite these progresses, the CUBIC series still take hours to clear millimeter-scale thick specimens [26,29]. A rapid and safe aqueous clearing method, specifically for tissues with millimeter-scale thickness, is still required.

To overcome this issue, a quantitative reagent screening method with clearing speed assessment ability is desired. The typical screening protocol is evaluating the clearing efficiency by visual inspection or light transmittance measurement of tissue sections or intact organs treated with candidate chemicals [11,24,29]. This method is time-and sample-consuming, labor-intensive, and is usually subject to artifacts. To address these issues, Ueda and colleagues developed a new evaluation protocol that uses homogenized tissue suspension instead of tissue sections or intact organs for chemical screening [26,33]. This method enables high-throughput, reproducible, and quantitative evaluation of reagent clearing efficiency and greatly reduces the number of animals or specimens used [26,33]. However, the tissue permeability of chemicals, which is a determinant of clearing speed, cannot be assessed using tissue suspension. Moreover, both aforementioned methods measure light transmittance at a certain time point after clearing. The results cannot be used to accurately quantify the clearing speed, especially for ultrafast clearing reagents. Thus, a method for real-time monitoring and quantification of the dynamic clearing process is desired to facilitate the development of rapid optical clearing methods.

In this study, we proposed a simple and economical screening method to meet this demand. The method quantifies the clearing speed based on real-time light transmittance measurement using a commercially available microplate reader. Porcine small intestine tissues used as testing samples were incubated in the candidate chemicals for measurement. A total of 12 different recipes can be simultaneously tested. Using this method, an updated CUBIC protocol, termed F-CUBIC (adding formamide to CUBIC), was developed. F-CUBIC rapidly clarifies millimeter-scale thick tissues within 2–20 min by simple immersion with negligible distortion even for long-term incubation ($\geq$7 days). It also provides good compatibility with fluorescent proteins and various staining techniques. Based on human colon specimens with mucosal hyperplasia, we demonstrated F-CUBIC is promising for use in 3D histopathological analysis of endoscopic biopsy specimens by combining with appropriate staining techniques. The proposed chemical screening method for rapid clearing and the optimized aqueous clearing protocol, F-CUBIC, will potentially benefit biomedical studies, especially the development of instant 3D histopathological diagnosis techniques.

2. Materials and methods

2.1. Mice and mouse sample preparation

6–8 weeks old C57BL/6J, Thy1-GFP-M (strain name: Tg(Thy1-EGFP)MJrs/J), and $CX_3CR\text{-}1^{GFP}$ (strain name: B6.129P2(Cg)-Cx3cr1tm1Litt/J) mice were used in this study. All mouse husbandry and experimental procedures were conducted in compliance with the policies approved by the

Biomedical Optics EXPRESS

Guangdong Provincial Animal Care and Use Committee and following the guidelines of the Animal Experimentation Ethics Committee of Shenzhen Institute of Advanced Technology, Chinese Academy of Sciences.

The mice were deeply anesthetized using sodium pentobarbital (150–200 μL of 1% w/v) through intraperitoneal injection, and then transcardially perfused with phosphate buffered saline (PBS) followed by 4% (w/v) paraformaldehyde (PFA) in PBS for fixation. Then, the intact brains and desired internal organs (including lung, intestine, kidney, thymus, heart, stomach, and spleen) were excised and subjected to post-fixation treatment in 4% PFA/PBS(-) overnight at 4 °C. Finally, the organs were sectioned into slices of millimeter-scale thickness using brain and tissue matrices or used directly for further experiments.

2.2. Human gastrointestinal specimens

Human intestine and gastric antrum samples beside pathological tissues, as well as transverse colon tissue with mucosal hyperplasia, were collected from Peking University Shenzhen Hospital (Shenzhen, China) through gastrointestinal endoscopy or surgery with patient consent. In all cases, the clinical diagnosis was confirmed by standard histopathological examination using half of each specimen. The remaining half was cleaned with PBS several times, and then fixed with 4% PFA/PBS(-) at 4 °C overnight for subsequent optical clearing, staining, and imaging. All experimental procedures were performed under the supervision and approval of the Ethics Committee for Human Research, Peking University Shenzhen Hospital (Ethics Approval No. 1427611284372).

2.3. Porcine small intestines

Porcine small intestines were purchased from a nearby supermarket, cleaned with PBS several times, and then fixed with 4% PFA/PBS(-) at 4 °C overnight. Afterwards, the intestines were opened and cut into 2×2 cm^2 pieces for quantitative reagent screening.

2.4. Quantitative screening of rapid optical clearing reagents

For rapid and quantitative screening of optical clearing reagents, we proposed a clearing efficiency assessment method based on quantifying the dynamic clearing process using a microplate reader (Fig. 1). The porcine small intestine was used as the test sample to fairly compare different reagents, since the porcine intestinal wall is almost laterally homogenous in structure and components (despite the axial layered structure) and the tissue can be easily obtained in large amounts. Specifically, a piece of 2×2 cm^2 porcine intestinal wall was placed into a custom-designed holder (Fig. 1(a)), and then the holder was placed into a well of a 12-well plate filled with 2 mL optical clearing reagent (Fig. 1(b)). By repeating the procedure, a total of 12 reagents can be prepared for simultaneous testing. Afterwards, the 12-well plate was placed into a microplate reader (Infinite M1000 PRO, Tecan) to record light transmittance over time. By fitting an exponential model,

$$Tr(t) = a - e^{-v(t-b)},$$

to the transmittance data, a constant parameter, v, was derived to quantify the clearing speed of different optical clearing reagents, where Tr and t are the transmittance and time, respectively, and a and b are two other constant parameters that need to be determined (Fig. 1(c)).

2.5. F-CUBIC protocols

F-CUBIC was optimized from CUBIC based on the quantitative screening method described in Section 2.4, and a total of six chemicals were screened, including mannose (Macklin, D813082), polyethylene glycol (PEG) 400 (Sigma-Aldrich, P3265), formamide (Sigma-Aldrich,

Biomedical Optics EXPRESS

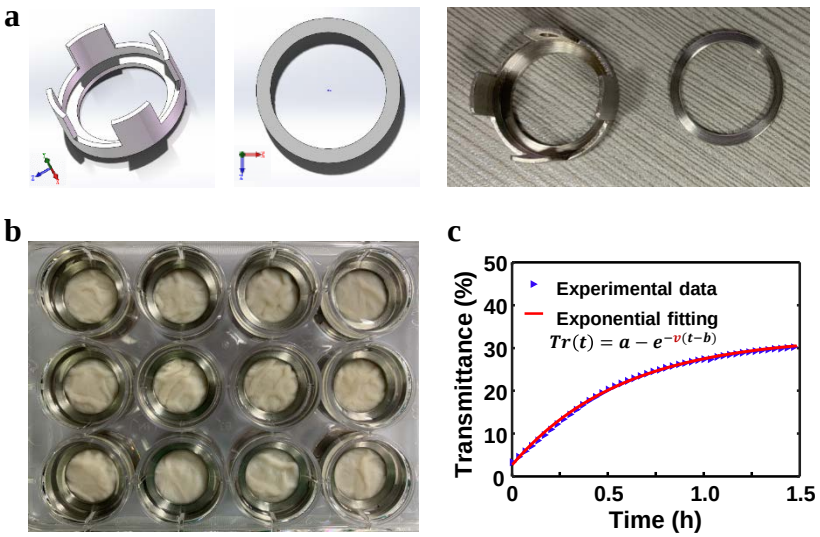

Fig. 1. Method for screening chemicals for rapid optical clearing. Porcine small intestine tissue was used as the testing sample and its light transmittance was measured in real time by a microplate reader during clearing. (a) Sample holder. (b) A total of 12 reagents can be simultaneously tested using a 12-well plate. (c) A parameter, v, is derived from exponential fitting of the transmittance curve to quantify the clearing speed of candidate reagent.

F9037), xylose (Macklin, X6221), ethanol (Macklin, E809056), and 1,2-propanediol (Sigma-Aldrich, V900115). Significantly, the recently developed one-step ultrafast clearing method for tissue slices, FOCM [30% (wt/vol) urea (Sigma-Aldrich, 15604), 20% (wt/vol) D-sorbitol (Macklin, S6169), and 5% (wt/vol) glycerol (Macklin, G810575) dissolved in DMSO (Macklin, D806647)] [31], was taken as the control in the chemical screening. The finalized F-CUBIC consisted of 10 wt% formamide and Sca*l*eCUBIC-1 [25 wt% urea, 25 wt% N,N,N',N'-tetrakis (2-hydroxypropyl)ethylenediamine (Beijing Budweiser, 230893), and 15 wt%Triton X-100 (Sigma-Aldrich, 10789704001)] [26] (generally shortened to CUBIC-1). For optical clearing, the fixed tissues were directly immersed in F-CUBIC with gentle shaking at room temperature. The incubation time was 2–20 min for mouse tissue sections and intact internal organs with a thickness of millimeter scale. For the whole mouse brain, the clearing time was extended to a week or longer, with the clearing reagent refreshed every 2-3 days. Samples requiring labeling were cleared along with staining, and the details are provided in the staining section. We emphasized recommendation of clearing millimeter-scale thick slices with F-CUBIC rather than large tissue blocks.

2.6. Tissue optical clearing with other clearing methods

The clearing methods, including CUBIC-1 [26] and Sca*l*eA2 [4M urea, 10% (wt/vol) glycerol, and 0.1% (wt/vol) Triton X-100] [22] were used for comparison with F-CUBIC. For optical clearing with these methods, the fixed tissues were directly immersed in clearing reagents and incubated under the same conditions as F-CUBIC clearing.

2.7. Staining

Staining of tissues requiring labeling was performed along with clearing at room temperature. For the human intestine, mouse intestine, and mouse lung samples, the fixed tissues were first immersed in F-CUBIC for two days, and then washed with PBS several times. Afterwards,

Biomedical Optics EXPRESS

the tissues were incubated with fluorescent dyes or fluorescent-labeled antibodies diluted in 0.1% (v/v) Triton X-100/PBS for three days. After staining, the tissues were washed with PBS again, incubated in F-CUBIC for 0.5 h, and then used for imaging. Here, the human intestinal specimen was stained with Alexa Fluor 488-conjugated phalloidin (1:50 dilution, Thermo Fisher Scientific, A12379) to label F-actin. The mouse intestine and lung samples were stained with Alexa Fluor 488-conjugated anti-alpha smooth muscle actin (α-SMA) antibody (1:50 dilution, Abcam, ab202295) to label actin.

For human gastric antrum specimens as well as transverse colon specimens with mucosal hyperplasia, the fixed tissues were immersed in F-CUBIC with 50 nM DAPI (Thermo Fisher Scientific, D3571) for one day to conduct optical clearing and nuclear staining simultaneously. Subsequently, the tissues were washed with PBS and used for imaging.

2.8. Two-photon excitation fluorescence microscopy

For fluorescence imaging, an upright two-photon microscope system (A1R-MP, Nikon) equipped with a Ti: sapphire laser (MaiTai eHP DeepSee, Spectra Physics) and a 25×, 1.1 NA water-immersion objective (N25X-APO-MP, Nikon) was used. The excitation wavelength was 780 nm for DAPI and 900 nm for the other labels. To prevent photodamage, the power on the sample was maintained below 40 mW. During imaging, the sample was kept submerged in optical clearing reagents or PBS and covered with a glass coverslip to block it from the immersion media of the objective. For 3D image visualization, Imaris (Version 7.6, Bitplane AG) and ImageJ (Version 1.51n, National Institutes of Health) were used.

2.9. Quantifications

***Brain size change quantification*:** The expansion or shrinkage of the brain was quantified based on bright-field images. First, the brain area in the image was measured by outlining it using the "freehand selections" function of ImageJ, after which the area of cleared brains was normalized to the area of uncleared ones and the linear expansion value was calculated as the square root of the normalized area to quantify brain size change [18].

***Imaging depth quantification*:** The imaging depth before and after clearing was quantified based on two-photon imaging of brain tissue with green fluorescent protein (GFP)-labeled neurons or microglia. As previously reported [18], the imaging depth was measured as the distance between the tissue surface and the plane where the last identifiable cell was located.

2.10. Statistical analysis

Statistical analyses were performed using GraphPad Prism version 5 (GraphPad Software). Data are presented as mean ± SEM. Comparisons between the two groups were performed using a two-tailed paired *t-test*. Comparisons between more than two groups were performed using one-way ANOVA followed by Tukey's multiple comparison test. Differences were considered statistically significant at $p < 0.05$.

3. Results and discussion

3.1. F-CUBIC: optimized from CUBIC by quantifying the dynamic clearing process

To facilitate chemical screening for rapid optical clearing, we proposed a simple and economical method with batch processing capability for clearing speed assessment and comparison. The method simultaneously measures the light transmittances of porcine small intestine tissues incubated in 12 different clearing reagents in real time using a microplate reader and takes v, which is calculated from the exponential fitting of each transmittance curve as an indicator of clearing speed (please refer to Section 2.4 for details). As the wall of porcine small intestine is almost laterally homogenous in structure and components (despite the axial layered structure),

Biomedical Optics EXPRESS

using it rather than other tissues or organs as the testing sample ensures a fair comparison. On the other hand, as one intestine is sufficient for numerous testing experiments, using it makes the test more ethical and economical. Moreover, by directly using actual tissues instead of homogenized tissue suspensions [26,33], the method retains the ability to evaluate chemical permeability, which is a determinant of the clearing speed. In addition, the millimeter-scale thickness of porcine small intestine wall matches our screening requirement for future endoscopic histological examination.

Utilizing the proposed method, we attempted developing a rapid and safe clearing protocol for 3D imaging of millimeter-scale thick tissues by optimizing the classical aqueous clearing method CUBIC [26]. This protocol was chosen because of its efficient clearing ability, favorable fluorescence compatibility, and widespread use [5,26]. CUBIC clearing is a two-step procedure. CUBIC-1 acts for delipidation, decolorization, and hydration, while Sca*l*eCUBIC-2 (generally shortened to CUBIC-2) acts mainly for RI matching. The drawbacks of the original CUBIC protocol mainly include modest clearing speed, tissue distortion of first swelling and then shrinking, as well as extra labor and time costs of the two-step procedure [26,29]. We consider replacing CUBIC-2 with other chemicals and developing an updated one-step CUBIC protocol for simple and rapid clearing. Taking the recently developed one-step ultrafast clearing method for tissue slices, FOCM [31], as the control for comparison, six commonly used chemicals with superior water solubility, low toxicity, high RI, and low molecular weight were chosen for screening, including formamide, mannose, polyethylene glycol (PEG) 400, xylose, ethanol, and 1,2-propanediol. The results showed that formamide had the fastest clearing speed among these chemicals when combined with CUBIC-1, and even remarkably faster than the FOCM (Fig. 2(a) and 2(b)). Furthermore, we tested different concentrations of formamide and found that 5 wt% formamide mixed with CUBIC-1 exhibited remarkably slower clearing speed, while the performances of other concentrations, including 10 wt%, 15 wt%, and 20 wt%, were similar (Fig. 2(c) and 2(d)). Therefore, we finalized an optimized protocol, termed F-CUBIC, as a mixture of 10 wt% formamide and CUBIC-1. The F-CUBIC has an RI of 1.44, close to the glycerol-containing CUBIC-2 (RI: 1.45–1.46 [26]).

To demonstrate the performance of F-CUBIC, we used Sca*l*eA2 [22], which is the most representative aqueous clearing method with simple immersion, for comparison, in addition to CUBIC-1. Similar to CUBIC-1 and Sca*l*eA2, F-CUBIC is also colorless and permissive to visible and near-infrared light (400–900 nm) with a transmittance of 80%–90% (Fig. 3(a)). By measuring the transmittance curves (Fig. 3(b) and 3(c)) and v values (Fig. 3(d)) on porcine small intestine tissues as mentioned above, F-CUBIC showed substantially better clearing efficiency and significantly faster clearing speed than CUBIC-1 and Sca*l*eA2.

The original CUBIC-1 was a mixture of 25 wt% urea, 25 wt% N,N,N',N'-tetrakis(2-hydroxypropyl)ethylenediamine, and 15 wt% Triton X-100 [26]. The enhanced clearing ability of F-CUBIC relative to CUBIC-1 might be due to the synergetic effect of formamide with urea and Triton X-100. Specifically, formamide is a small, uncharged molecule bearing both hydrogen donor and acceptor groups as urea, and thus has a strong permeability and hyperhydration ability. These abilities can induce molecular flux across cell membranes and solve proteins by disturbing their hydrogen-bonding networks [10]. Moreover, it is more permeable because of its lower molecular weight (with one less NH_2 group) and has a much higher RI (1.45 [10]) than urea (with an RI of 1.40 [11]). Additionally, formamide can solubilize lipids [10]. Compared with formamide, urea has a much higher hydration energy because of the strong synergetic effect of the two NH2 groups and Triton X-100 has a stronger delipidation ability [10]. F-CUBIC combines the strengths of formamide, urea, and Triton X-100 and results in more effective and faster tissue clearing.

Biomedical Optics EXPRESS

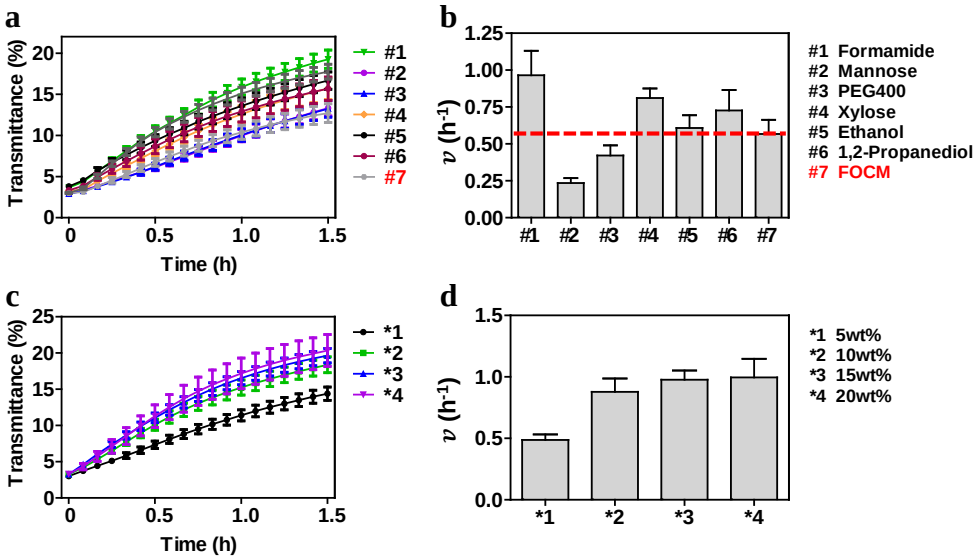

Fig. 2. Development of F-CUBIC by quantitative chemical screening. (a, b) Light transmittance curves and corresponding v values measured for different recipes each consist of 10 wt% candidate chemical and CUBIC-1. Formamide with CUBIC-1 achieves the fastest clearing. (c, d) Further determining the concentration of formamide. The error bars denote the SEM.

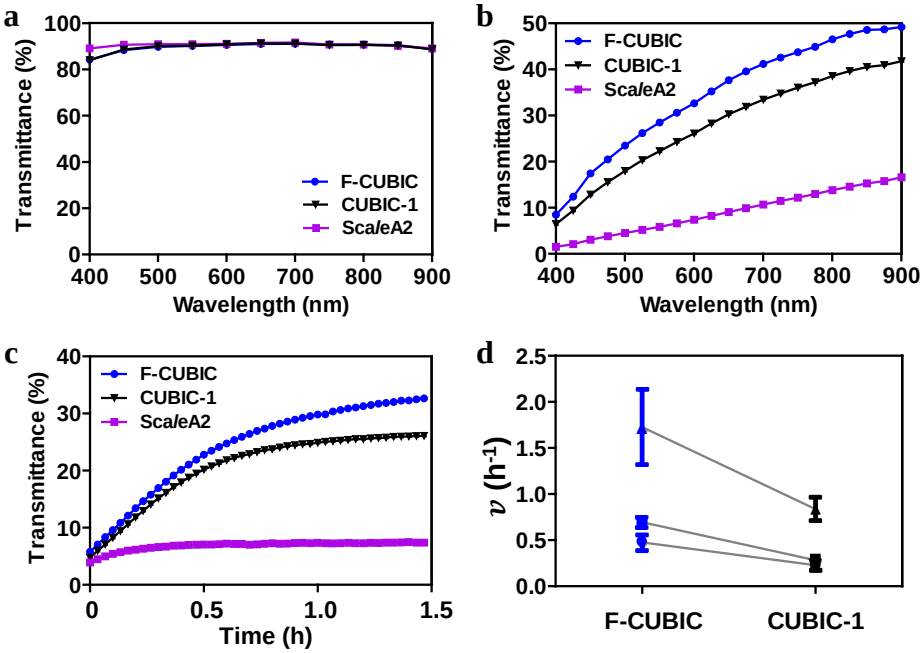

Fig. 3. F-CUBIC achieves more efficient and faster clearing than CUBIC-1 and Sca*l*eA2. (a) Light transmission curves of the three clearing reagents. (b, c) Light transmission curves of the porcine small intestine tissues treated with these reagents. (a) and (b) were measured over wavelength, and (b) was measured at 2 h after treatment. (c) was measured over time within 1.5 h. (d) v values of F-CUBIC compared with CUBIC-1. The error bars denote the SEM.

Biomedical Optics EXPRESS

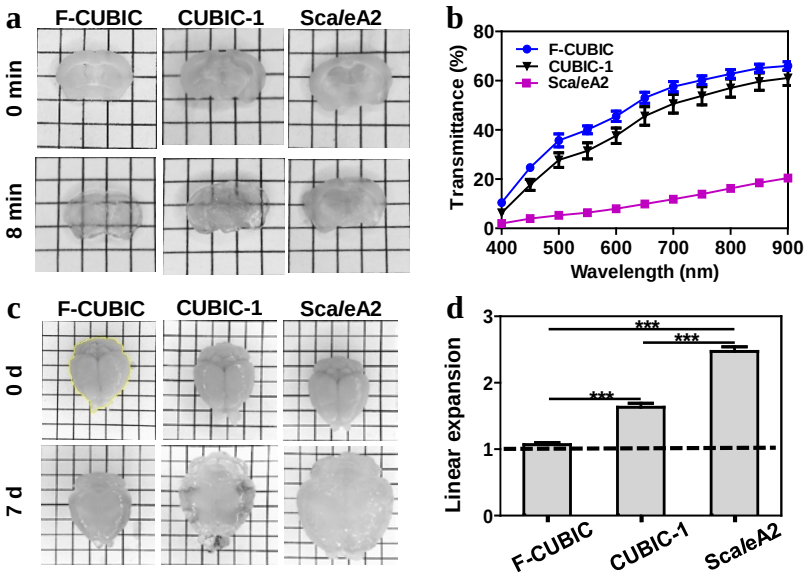

Fig. 4. F-CUBIC rapidly clarifies mouse brain tissues with negligible distortion, compared with CUBIC-1 and Sca*l*eA2. (a, b) 1.5-mm-thick brain slices after treatment with the three reagents at room temperature for 8 min (a) and corresponding light transmittance measured over wavelength (b). Images of samples before clearing were also provided for comparison (a). (c, d) Intact adult mouse brains before and after treatment with the above reagents for 7 days (c) and sample distortion measured accordingly (d, n = 3). As indicated by the yellow line, the brain was outlined for area measurement and linear expansion calculation (c). ***: $P < 0.001$, one-way ANOVA followed by Tukey's multiple comparison test (d). The error bars denote the SEM (b, d).

3.2. *F-CUBIC enables rapid clearing of various tissues with negligible distortion*

In the reagent-screening experiment described above, the clearing efficiency of F-CUBIC has only been tested on porcine small intestines. To further examine the universal adaptability of F-CUBIC, we implemented it in various other tissues. For 1.5-mm-thick mouse brain slices incubated for 8 min, F-CUBIC made the sample extremely transparent compared to CUBIC-1 and Sca*l*eA2 (Fig. 4(a) and 4(b)). CUBIC-1 only partially cleared the lipid-rich white matter, and Sca*l*eA2 showed no clearing effect on both gray and white matter (Fig. 4(a) and 4(b)). In addition, negligible tissue expansion was observed in intact mouse brains after F-CUBIC treatment, even after incubating for one week. This might be because the urea-hydration-induced tissue swelling was adequately balanced with osmotic dehydration-induced tissue shrinkage. In contrast, the samples were significantly swollen by CUBIC-1 and Sca*l*eA2 treatment, with a linear expansion of 1.5-2.6 times (Fig. 4(c) and 4(d)). Additional examples of different tissue slices with millimeter-scale thickness treated with F-CUBIC are shown in Fig. 5. A high level of tissue transparency was achieved within 2–20 min without obvious distortion.

In addition to the ultrafast FOCM (Fig. 2(a) and 2(b)) and the representative CUBIC-1 and Sca*l*eA2 (Figs. 3 and 4), we also investigated the clearing speed of other existing aqueous clearing methods, including SeeDB/SeeDB2 [24,25], the entire CUBIC [26,27], UbasM [29], Sca*l*eS [32], MACS [11], RTF [30], etc., for millimeter-thick tissues by reviewing papers. Although CUBIC, UbasM, and MACS showed relative faster clearing speed among these methods [11,24–27,29,30,32], they are still slower than F-CUBIC. CUBIC and UbasM cleared 1-mm-thick brain slice with 1-2 h [29]. MACS cleared 1-mm- and 2-mm-thick brain slices

Biomedical Optics EXPRESS

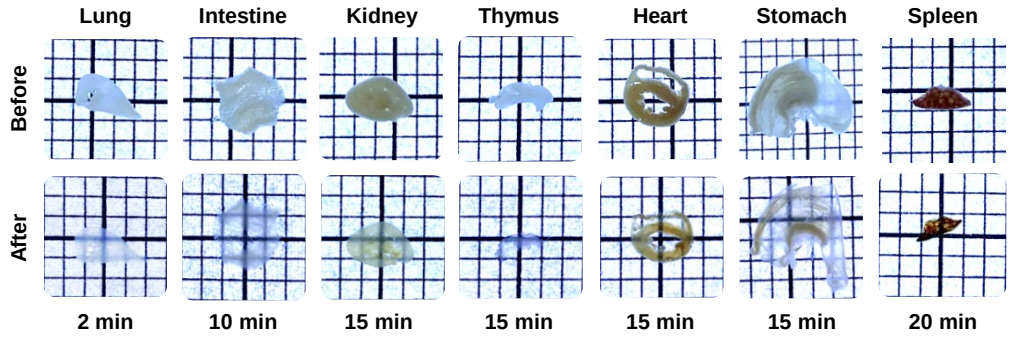

Fig. 5. F-CUBIC provides rapid and versatile clearing of millimeter-thick tissues (from 6-week-old mice). In terms of lung, kidney, heart, and spleen, 1-mm-thick slices were prepared; while for intestine and stomach, the tissues were cut open to expose the inner wall for clearing; for thymus, the intact organ was directly cleared.

with 0.5 h and 6h, respectively [11]. Besides, the three methods are all multi-step protocols. In contrast, F-CUBIC cleared 1.5-mm-thick brain slice with only 8 min (Fig. 4(a)) and other millimeter-thick tissues with 2–20 min (Fig. 5) by one-step immersion. As this study focuses on rapid one-step clearing protocols, and the clearing speed of F-CUBIC is even faster than the first step of the above methods, we didn't take them into experimental comparison.

3.3. *F-CUBIC significantly improves imaging depth and contrast while providing favorable fluorescent-protein compatibility*

As F-CUBIC achieves rapid optical clearing with negligible tissue distortion and universal adaptability, we further considered its practical value in deep-tissue imaging. Using a two-photon microscope system (A1R-MP, Nikon), brain slices with GFP-labeled neurons or microglial cells (from Thy1-GFP-M and $CX_3CR\text{-}1^{GFP}$ mice, respectively) were imaged before clearing and after F-CUBIC treatment for ~20 min (Fig. 6). A slice thickness of 3 mm was chosen to cover the maximum imaging depth of the imaging system (namely the working distance of the objective, which is 2 mm).

A detailed image comparison obtained at superficial layers before and after clearing was first performed and extremely similar cell morphologies were observed (Fig. 6(a), 6(b), 6(d), and 6e), indicating that F-CUBIC has favorable fluorescent-protein compatibility. Furthermore, imaging depth and quality were evaluated. With F-CUBIC clearing, the maximum penetration depth of neuron imaging increases from 230 μm to 1.06 mm on average, achieving a nearly five-fold improvement (Fig. 6(a)-(c)), and the fine structures of axons and dendrites can be clearly identified even at depths > 1 mm (red dashed boxes in Fig. 6(a)). However, details and even the soma severely blurred at > 200-μm depth before clearing (yellow dashed boxes in Fig. 6(b)). Similar conclusions were obtained for microglial imaging. The average imaging depth increases from 220 μm to 1.05 mm after clearing (Fig. 6(d)-(f)), and the microglial processes were clearly observed till depths > 740 μm (red dashed boxes in Fig. 6(d)).However, the processes were severely lost at > 200-μm depth without clearing (yellow dashed boxes in Fig. 6(e)). These results demonstrate that F-CUBIC can substantially facilitate high-resolution deep-tissue fluorescence imaging by short-term immersion.

Notably, the immersion media of the objective that we used in the imaging system is water, which has a refractive index (RI) of 1.33, while the RI of F-CUBIC is 1.44. For two-photon imaging of optical cleared specimens, the RI mismatch between the objective immersion media and the clearing reagent induces spherical aberration (SA), causing significant degradation of

Biomedical Optics EXPRESS

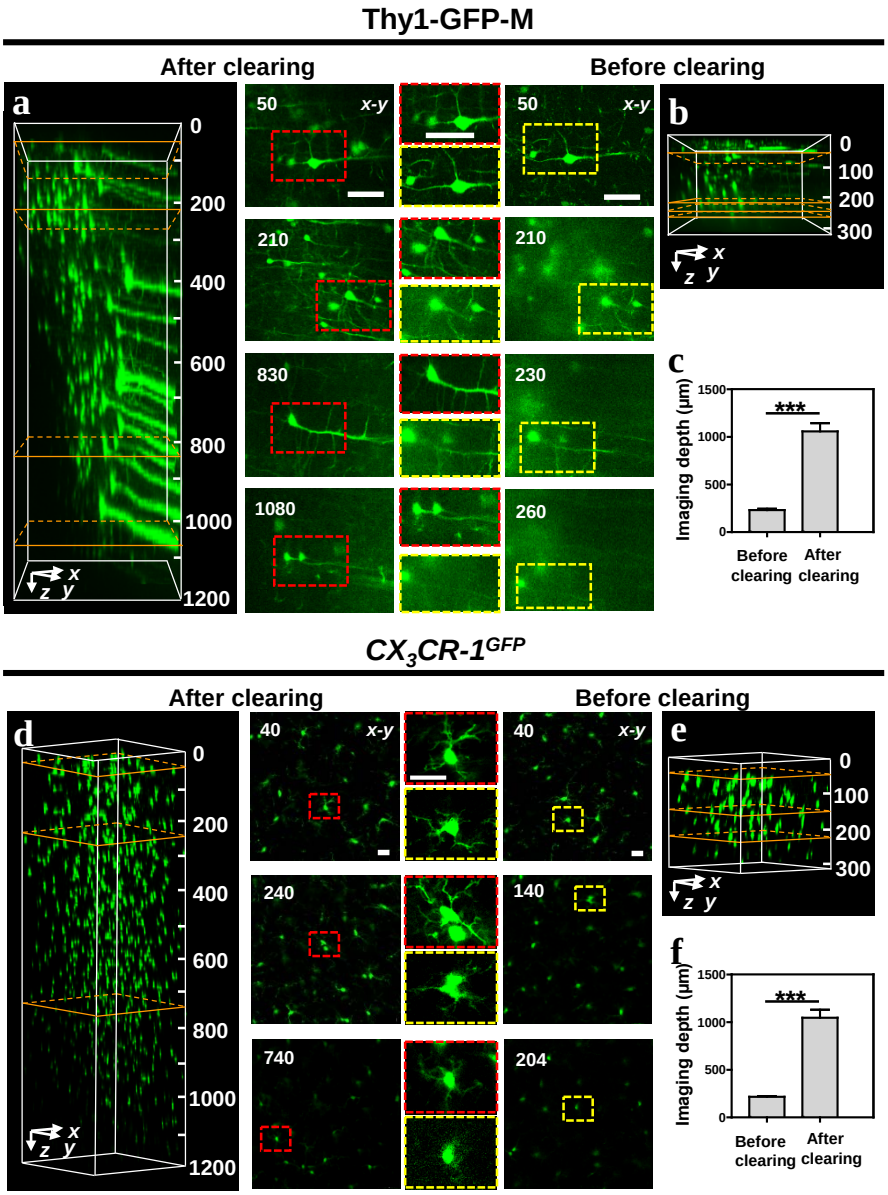

Fig. 6. F-CUBIC improves fluorescence imaging depth and quality. (a-c) Images of a 3-mm-thick brain slice from adult Thy1-GFP-M mouse before (b) and after F-CUBIC clearing for ~20 min (a) and imaging depths measured accordingly (c, n = 3). The fluorescence signal is from GFP-labeled neurons. (d-f) Images of a 3-mm-thick brain slice from adult $CX_3CR\text{-}1^{GFP}$ mouse before (e) and after F-CUBIC clearing for ~20 min (d) and imaging depths measured accordingly (f, n = 3). The fluorescence signal is from GFP-labeled microglial cells. Images with different depths and magnified views of the boxed areas (the middle columns) were presented along with 3D images (the far left and right columns). The depth is labeled in the top left corner of each panel and the unit is μm (a, b, d, e). Scale bars, 50 μm in (a, b) and 20 μm in (d, e). The error bars denote the SEM. ***: $P < 0.001$, two-tailed paired t test (c, f).

Biomedical Optics EXPRESS

imaging depth [35]. Combining SA correction with F-CUBIC clearing would further improve the imaging depth and quality [35].

3.4. F-CUBIC is compatible with dye staining and immunohistochemistry staining

With the exception of fluorescent proteins, fluorescent labeling with dyes or immunostaining is highly valuable and commonly used for high-lighting molecules of interest in many studies, such as histopathological analysis. To examine F-CUBIC's compatibility with fluorescent staining, we performed fluorescent-dye staining and immunostaining on clinical specimens and animal samples along with F-CUBIC clearing. Alexa Fluor 488-conjugated phalloidin and antibody were used to label F-actin in human intestine specimens and actin in mouse intestine and lung samples, respectively. DAPI was used to stain nuclei in the human gastric antrum

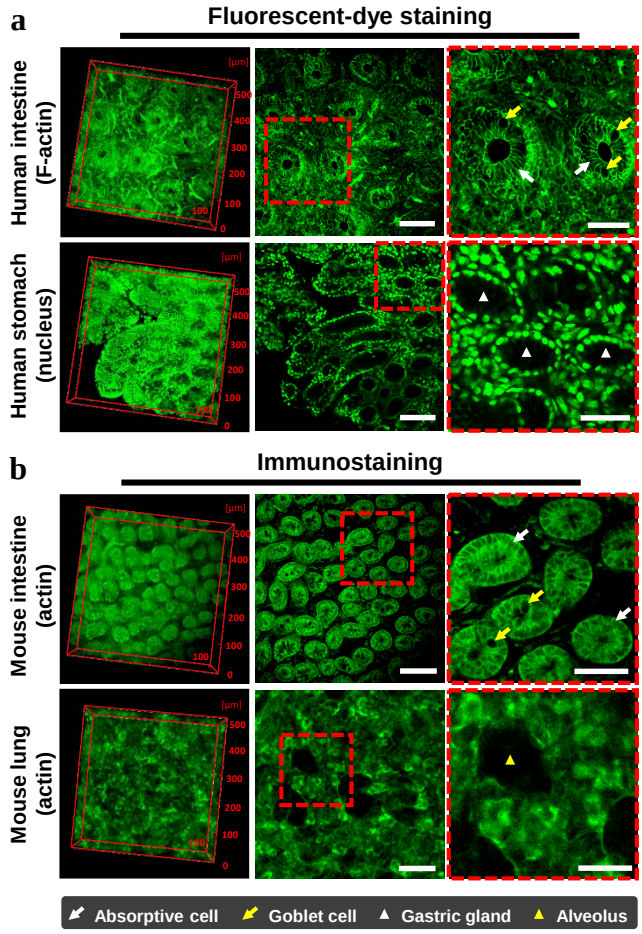

Fig. 7. F-CUBIC is compatible with various staining techniques. (a) Images of human intestine and gastric tissues labeled with Alexa Fluor 488-conjugated phalloidin and DAPI, respectively. (b) Images of mouse intestine and lung samples labeled with Alexa Fluor 488-conjugated anti-α-SMA antibody. F-CUBIC clearing was performed along with staining. Images at a certain depth (the middle column; scale bars, 100 μm) and magnified views of the boxed areas (the right column; scale bars, 50 μm) were presented along with 3D images (the left column).

Biomedical Optics EXPRESS

specimens. Two-photon imaging results showed that the intestinal glands, lined with simple columnar epithelium, were clearly identified within the lamina propria of both human and mouse intestinal mucosae (the first row of Fig. 7(a) and 7(b)). The absorptive and goblet cells (indicated with white and yellow arrows, respectively, in Fig. 7(a) and 7(b)) that constitute the epithelium were easily discriminated. In addition, gastric glands that are circular or ovoid in cross-section and closely packed side-by-side (indicated with white triangles in Fig. 7(a)) within the lamina propria of human gastric antrum specimens were observed according to the neatly arranged nuclei, and the alveoli (indicated with yellow triangles in Fig. 7(b)) were normally presented in the mouse lung sample. These observations are highly consistent with the typical histological morphology of corresponding tissues [36,37], indicating that the fluorescent labels were successfully maintained along with F-CUBIC clearing. As a high concentration of

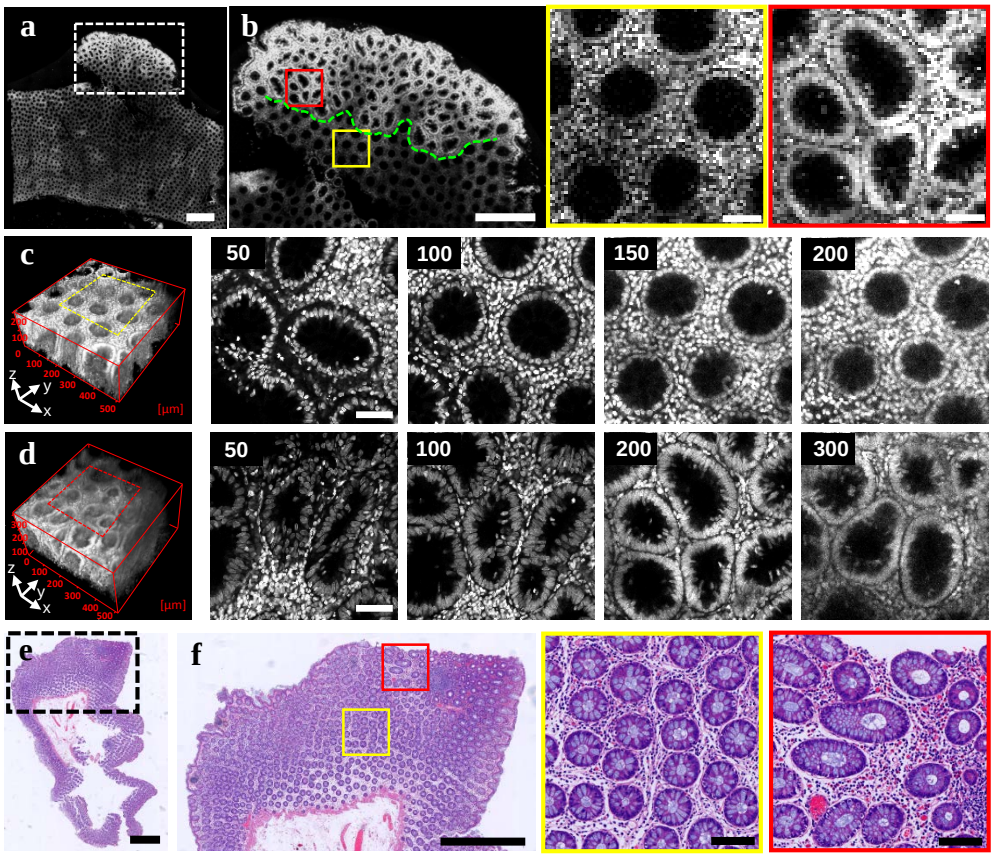

Fig. 8. F-CUBIC combined with two-photon microscopy allows nondestructive 3D histopathological imaging of endoscopic human colon specimen. (a) The large-field-of-view image of human transverse colon tissue with mucosal hyperplasia. (b) Magnified view of the boxed area in (a). The green dashed line roughly delineates the boundary between normal and diseased areas. Representative normal and diseased areas marked with yellow and red boxes, respectively, were further magnified. (c, d) 3D images and 2D images with different depths of the boxed areas in (b). The depth is labeled in the top left corner of each panel and the unit is μm. (e) H&E stained histology images of neighboring specimen. (f) Magnified view of the boxed area in (e), and representative normal and diseased areas marked with yellow and red boxes, respectively, were further magnified. Scale bars, 1 mm in (a, e) and the left images in (b, f); 100 μm in (c, d) and the middle and right images in (b, f).

Biomedical Optics EXPRESS

formamide is incompatible with immunohistochemistry and genetically encoded fluorescence proteins [23], decreasing its concentration to 10 v/v% may ensure that F-CUBIC could inherit the favorable fluorescent-labeling compatibility of CUBIC.

3.5. F-CUBIC facilitates 3D histopathology of endoscopic biopsy specimens

We further assessed the feasibility of combining F-CUBIC with two-photon microscopy for slide-free nondestructive biopsy. Here, an endoscopic biopsy specimen, the human transverse colon tissue with mucosal hyperplasia, was tested. For highlighting histological morphology of the tissues, nuclear staining with DAPI was performed along with F-CUBIC clearing. Using the two-photon microscopy, the 3D structure of the mucosal lamina propria occupied by closely packed glands was presented (Fig. 8(a)–8(d)). The normal mucosal glands are uniformly distributed with circular shapes and similar sizes (yellow boxed region in Fig. 8(b) and 8(c)), while the glands within the hyperplasia area have irregular shape and heterogeneous size (red boxed region in Fig. 8(b), Fig. 8(d)). These findings are consistent with observations from H&E stained histological images (Fig. 8(e)–8(f)), indicating that F-CUBIC would significantly benefit slide-free nondestructive biopsy.

4. Conclusion

We proposed a simple and economical method that provides quantitative monitoring of the dynamic clearing process for screening rapid optical clearing reagents. By using a commercially available microplate reader and a 12-well plate, the proposed method allows real-time light transmittance measurement of samples incubated in 12 candidate recipes in a single test. From the obtained transmittance curve, an indicator that quantifies the clearing speed can be derived. Porcine small intestine tissues of the same size as the testing samples were chosen as they ensured a fair, ethical, and economical screening, allowed tissue permeability evaluation of chemicals, and matched our screening requirement of clearing millimeter-scale thick tissues. Notably, the testing samples were not restricted to porcine small intestine, any tissue was available depending on the purpose of chemical screening. In this study, screening using the proposed method resulted in an updated CUBIC protocol called F-CUBIC. Depending on the synergetic effect of formamide with urea and Triton X-100, F-CUBIC allows effective, fast (2-20 min), and versatile clearing of millimeter-scale thick tissues with negligible tissue distortion by simple immersion at room temperature. Moreover, favorable compatibility of F-CUBIC with fluorescent proteins and various staining techniques was demonstrated in both clinical specimens and animal samples. Finally, we successfully validated the feasibility of combining F-CUBIC with optical sectioning microscopy for slide-free nondestructive biopsy based on an endoscopic human colon specimen with mucosal hyperplasia. In summary, the proposed method that allows real-time quantification of the dynamic clearing process, as well as the optimized aqueous clearing protocol, F-CUBIC, may prove invaluable in biomedical research and clinical applications involving rapid 3D mapping of tissues, such as instant 3D histopathological diagnosis. However, our method also has some limits. For example, the proposed chemical screening method only allows comparison of data measured from the same porcine small intestine. Because the thickness of intestinal wall varies greatly from one to another among pigs due to the differences in age. Besides, the method was designed for screening one-step clearing protocols. For multi-step clearing, adding reagents during real-time transmittance measurement may induce large data perturbation. In future, we will attempt to improve the method to overcome these problems. On the other hand, in addition to clearing and imaging techniques, rapid 3D tissue mapping is also substantially hindered by the time-consuming thick-tissue staining protocol. In this study, the penetration depth of staining in biological tissues is only ~100 μm to ~300 μm even after incubating for 1–3 days (as shown in Figs. 7 and 8). Why it is so low is unclear so far. For immunostaining, it seems that the large molecular weight of antibodies is a major limiting factor. Selecting fluorescent

Biomedical Optics EXPRESS

dyes with low molecular weight and optimizing the staining conditions, such as evolving physical penetration-enhancing strategies, may be helpful to speed up staining and extend the penetration depth. In the future, we will attempt to develop rapid staining techniques synergistic with F-CUBIC clearing based on these strategies to satisfy many more possible applications.

Funding. National Key Research and Development Program of China (2017YFC0110200); National Natural Science Foundation of China (81822023, 82071972, 91959121); Basic and Applied Basic Research Foundation of Guangdong Province (2019A1515011746, 2020A1515010675, 2020B121201010); Scientific Instrument Innovation Team of the Chinese Academy of Sciences (GJJSTD20180002); Shenzhen Basic Research Program (JCYJ20180507182432303, ZDSY20130401165820357).

Acknowledgments. We thank Prof. Yang Zhan (Brain Cognition and Brain Disease Institute, Shenzhen Institute of Advanced Technology, Chinese Academy of Sciences, Shenzhen, China) and Prof. Bo Peng (Institute for Translational Brain Research, Fudan University) for providing the Thy1-GFP-M and $CX_3CR\text{-}1^{GFP}$ mice, respectively.

Disclosures. The authors declare no conflicts of interest.

Data availability. Data underlying the results presented in this paper can be obtained from the authors upon request.

References

1. A. Y. Shih, J. D. Driscoll, P. J. Drew, N. Nishimura, C. B. Schaffer, and D. Kleinfeld, "Two-photon microscopy as a tool to study blood flow and neurovascular coupling in the rodent brain," J. Cereb. Blood Flow Metab. **32**(7), 1277–1309 (2012).
2. P. Fei, J. Nie, J. Lee, Y. Ding, S. Li, H. Zhang, M. Hagiwara, T. Yu, T. Segura, C.-M. Ho, D. Zhu, and T. K. Hsiai, "Subvoxel light-sheet microscopy for high-resolution high-throughput volumetric imaging of large biomedical specimens," Adv. Photonics **1**(1), 016002 (2019).
3. R. Tomer, M. Lovett-Barron, I. Kauvar, A. Andalman, V. M. Burns, S. Sankaran, L. Grosenick, M. Broxton, S. Yang, and K. Deisseroth, "SPED light sheet microscopy: fast mapping of biological system structure and function," Cell **163**(7), 1796–1806 (2015).
4. T. Yu, Y. Qi, H. Gong, Q. Luo, and D. Zhu, "Optical clearing for multiscale biological tissues," J. Biophotonics **11**(2), e201700187 (2018).
5. H. R. Ueda, H.-U. Dodt, P. Osten, M. N. Economo, J. Chandrashekar, and P. J. Keller, "Whole-brain profiling of cells and circuits in mammals by tissue clearing and light-sheet microscopy," Neuron **106**(3), 369–387 (2020).
6. M. Belle, D. Godefroy, C. Dominici, C. Heitz-Marchaland, P. Zelina, F. Hellal, F. Bradke, and A. Chedotal, "A simple method for 3D analysis of immunolabeled axonal tracts in a transparent nervous system," Cell Rep. **9**(4), 1191–1201 (2014).
7. I. Costantini, R. Cicchi, L. Silvestri, F. Vanzi, and F. S. Pavone, "In-vivo and ex-vivo optical clearing methods for biological tissues: review," Biomed. Opt. Express **10**(10), 5251–5267 (2019).
8. H. R. Ueda, A. Erturk, K. Chung, V. Gradinaru, A. Chedotal, P. Tomancak, and P. J. Keller, "Tissue clearing and its applications in neuroscience," Nat. Rev. Neurosci. **21**(2), 61–79 (2020).
9. K. R. Weiss, F. F. Voigt, D. P. Shepherd, and J. Huisken, "Tutorial: practical considerations for tissue clearing and imaging," Nat. Protoc. **16**(6), 2732–2748 (2021).
10. K. Tainaka, A. Kuno, S. I. Kubota, T. Murakami, and H. R. Ueda, "Chemical principles in tissue clearing and staining protocols for whole-body cell profiling," Annu. Rev. Cell Dev. Biol. **32**(1), 713–741 (2016).
11. J. Zhu, T. Yu, Y. Li, J. Xu, Y. Qi, Y. Yao, Y. Ma, P. Wan, Z. Chen, X. Li, H. Gong, Q. Luo, and D. Zhu, "MACS: rapid aqueous clearing system for 3D mapping of intact organs," Adv. Sci. **7**(8), 1903185 (2020).
12. A. Erturk, K. Becker, N. Jahrling, C. P. Mauch, C. D. Hojer, J. G. Egen, F. Hellal, F. Bradke, M. Sheng, and H. U. Dodt, "Three-dimensional imaging of solvent-cleared organs using 3DISCO," Nat. Protoc. **7**(11), 1983–1995 (2012).
13. D. S. Richardson and J. W. Lichtman, "Clarifying tissue clearing," Cell **162**(2), 246–257 (2015).
14. P. Ariel, "A beginner's guide to tissue clearing," Int. J. Biochem. Cell Biol. **84**, 35–39 (2017).
15. C. Pan, R. Cai, F. P. Quacquarelli, A. Ghasemigharagoz, A. Lourbopoulos, P. Matryba, N. Plesnila, M. Dichgans, F. Hellal, and A. Erturk, "Shrinkage-mediated imaging of entire organs and organisms using uDISCO," Nat. Methods **13**(10), 859–867 (2016).
16. R. Cai, C. Pan, A. Ghasemigharagoz, M. I. Todorov, B. Foerstera, S. Zhao, H. S. Bhatia, A. Parra-Damas, L. Mrowka, D. Theodorou, M. Rempfler, A. L. R. Xavier, B. T. Kress, C. Benakis, H. Steinke, S. Liebscher, I. Bechmann, A. Liesz, B. Menze, M. Kerschensteiner, M. Nedergaard, and A. Ertuerk, "Panoptic imaging of transparent mice reveals whole-body neuronal projections and skull-meninges connections," Nat. Neurosci. **22**(2), 317–327 (2019).
17. C. Hahn, K. Becker, S. Saghafi, M. Pende, A. Avdibasic, M. Foroughipour, D. E. Heinz, C. T. Wotjak, and H. U. Dodt, "High-resolution imaging of fluorescent whole mouse brains using stabilised organic media (sDISCO)," J. Biophotonics **12**(8), e201800368 (2019).
18. Y. Qi, T. Yu, J. Xu, Q. Luo, and D. Zhu, "FDISCO: advanced solvent-based clearing method for imaging whole organs," Sci. Adv. **5**(1), aau8355 (2019).
19. K. Chung and K. Deisseroth, "CLARITY for mapping the nervous system," Nat. Methods **10**(6), 508–513 (2013).

Biomedical Optics EXPRESS

20. K. Chung, J. Wallace, S. Y. Kim, S. Kalyanasundaram, A. S. Andalman, T. J. Davidson, J. J. Mirzabekov, K. A. Zalocusky, J. Mattis, A. K. Denisin, S. Pak, H. Bernstein, C. Ramakrishnan, L. Grosenick, V. Gradinaru, and K. Deisseroth, "Structural and molecular interrogation of intact biological systems," Nature **497**(7449), 332–337 (2013).
21. B. Yang, J. B. Treweek, R. P. Kulkarni, B. E. Deverman, C. K. Chen, E. Lubeck, S. Shah, L. Cai, and V. Gradinaru, "Single-cell phenotyping within transparent intact tissue through whole-body clearing," Cell **158**(4), 945–958 (2014).
22. H. Hama, H. Kurokawa, H. Kawano, R. Ando, T. Shimogori, H. Noda, K. Fukami, A. Sakaue-Sawano, and A. Miyawaki, "Sca*l*e: a chemical approach for fluorescence imaging and reconstruction of transparent mouse brain," Nat. Neurosci. **14**(11), 1481–1488 (2011).
23. T. Kuwajima, A. A. Sitko, P. Bhansali, C. Jurgens, W. Guido, and C. Mason, "Clear(T): a detergent- and solvent-free clearing method for neuronal and non-neuronal tissue," Development **140**(6), 1364–1368 (2013).
24. M. T. Ke, S. Fujimoto, and T. Imai, "SeeDB: a simple and morphology-preserving optical clearing agent for neuronal circuit reconstruction," Nat. Neurosci. **16**(8), 1154–1161 (2013).
25. M. T. Ke, Y. Nakai, S. Fujimoto, R. Takayama, S. Yoshida, T. S. Kitajima, M. Sato, and T. Imai, "Super-resolution mapping of neuronal circuitry with an index-optimized clearing agent," Cell Rep. **14**(11), 2718–2732 (2016).
26. E. A. Susaki, K. Tainaka, D. Perrin, F. Kishino, T. Tawara, T. M. Watanabe, C. Yokoyama, H. Onoe, M. Eguchi, S. Yamaguchi, T. Abe, H. Kiyonari, Y. Shimizu, A. Miyawaki, H. Yokota, and H. R. Ueda, "Whole-brain imaging with single-cell resolution using chemical cocktails and computational analysis," Cell **157**(3), 726–739 (2014).
27. K. Tainaka, S. I. Kubota, T. Q. Suyama, E. A. Susaki, D. Perrin, M. Ukai-Tadenuma, H. Ukai, and H. R. Ueda, "Whole-body imaging with single-cell resolution by tissue decolorization," Cell **159**(4), 911–924 (2014).
28. B. Hou, D. Zhang, S. Zhao, M. Wei, Z. Yang, S. Wang, J. Wang, X. Zhang, B. Liu, L. Fan, Y. Li, Z. Qiu, C. Zhang, and T. Jiang, "Scalable and DiI-compatible optical clearance of the mammalian brain," Front. Neuroanat. **9**, 19 (2015).
29. L. Chen, G. Li, Y. Li, Y. Li, H. Zhu, L. Tang, P. French, J. Mcginty, and S. Ruan, "UbasM: an effective balanced optical clearing method for intact biomedical imaging," Sci. Rep. **7**(1), 12218 (2017).
30. T. Yu, J. Zhu, Y. Li, Y. Ma, J. Wang, X. Cheng, S. Jin, Q. Sun, X. Li, H. Gong, Q. Luo, F. Xu, S. Zhao, and D. Zhu, "RTF: a rapid and versatile tissue optical clearing method," Sci. Rep. **8**(1), 1964 (2018).
31. X. Zhu, L. Huang, Y. Zheng, Y. Song, Q. Xu, J. Wang, K. Si, S. Duan, and W. Gong, "Ultrafast optical clearing method for three-dimensional imaging with cellular resolution," Proc. Natl. Acad. Sci. U. S. A. **116**(23), 11480–11489 (2019).
32. H. Hama, H. Hioki, K. Namiki, T. Hoshida, H. Kurokawa, F. Ishidate, T. Kaneko, T. Akagi, T. Saito, T. Saido, and A. Miyawaki, "Sca*l*eS: an optical clearing palette for biological imaging," Nat. Neurosci. **18**(10), 1518–1529 (2015).
33. K. Tainaka, T. C. Murakami, E. A. Susaki, C. Shimizu, R. Saito, K. Takahashi, A. Hayashi-Takagi, H. Sekiya, Y. Arima, S. Nojima, M. Ikemura, T. Ushiku, Y. Shimizu, M. Murakami, K. F. Tanaka, M. Iino, H. Kasai, T. Sasaoka, K. Kobayashi, K. Miyazono, E. Morii, T. Isa, M. Fukayama, A. Kakita, and H. R. Ueda, "Chemical landscape for tissue clearing based on hydrophilic reagents," Cell Rep. **24**(8), 2196–2210.e9 (2018).
34. T. C. Murakami, T. Mano, S. Saikawa, S. A. Horiguchi, D. Shigeta, K. Baba, H. Sekiya, Y. Shimizu, K. F. Tanaka, H. Kiyonari, M. Iino, H. Mochizuki, K. Tainaka, and H. R. Ueda, "A three-dimensional single-cell-resolution whole-brain atlas using CUBIC-X expansion microscopy and tissue clearing," Nat. Neurosci. **21**(4), 625–637 (2018).
35. Y. Gao, L. Liu, Y. Yin, J. Liao, J. Yu, T. Wu, S. Ye, H. Li, and W. Zheng, "Adaptive optics via pupil ring segmentation improves spherical aberration correction for two-photon imaging of optically cleared tissues," Opt. Express **28**(23), 34935–34947 (2020).
36. S. Zhang, *An Atlas of Histology* (Springer, New York, 1999), Chap. 10.
37. S. Zhang, *An Atlas of Histology* (Springer, New York, 1999), Chap. 9.